Robotics and Autonomous Systems 98 (2017) 15–29

Contents lists available at ScienceDirect

Robotics and Autonomous Systems

journal homepage: www.elsevier.com/locate/robot

Robust output feedback assistive control of a compliantly actuated knee exoskeleton

Iman Kardan, Alireza Akbarzadeh *

Center of Excellence on Soft Computing and Intelligent Information Processing, Mechanical Engineering Department, Ferdowsi University of Mashhad, Mashhad, Iran

HIGHLIGHTS

- A robust assistive controller is proposed for compliantly actuated exoskeletons.
- H_∞ analysis is used to define robust stability and robust performance constraints.
- The controller is evaluated through some simulations and real-world experiments.
- The controller has successfully reduced the loads on the knee muscles.

ARTICLE INFO

Article history:
Received 2 January 2017
Received in revised form 6 August 2017
Accepted 6 September 2017
Available online 20 September 2017

Keywords:
Exoskeleton
H_∞ robustness analysis
Output feedback assistive control method
Compliant actuation
Integral admittance

ABSTRACT

The use of compliant actuators in assistive exoskeletons offers an increased level of comfort for their users. Various control algorithms are presented for assistive exoskeletons, seeking to facilitate wearer's motions. This paper complements a newly proposed output feedback assistive control (OFAC) algorithm for compliantly actuated exoskeletons. H_∞ analysis is used to define robust stability and robust performance constraints for the OFAC method. The robust OFAC method is then implemented on a custom made knee exoskeleton. Effectiveness of the proposed method is demonstrated through some simulations and experiments. Robustness of the OFAC method is further verified by successful reduction of the required knee torques in the non-linear model of the human–exoskeleton system as well as decreasing the muscles activities in a healthy subject wearing the FUM-KneeExo. The OFAC method is independent from user intent, has a simple model free structure, requires a very low number of sensors and simplifies the assistive control objective into position control of the compliant actuator. Moreover, the OFAC method has a very low number of adjustable control parameters which simplifies the adaptation of the OFAC method to different users in real-world applications. The proposed OFAC method can be used as a building block in assistive control of compliantly actuated exoskeletons. This, along with the superior advantages of the proposed OFAC method, should potentially boost the increasing applications of compliant actuators in assistive exoskeletons.

1. Introduction

Exoskeletons are wearable robots that combine human intellect with machine power to increase the user's abilities and boost the machine intellect. These robots are generally classified in three main categories of assistive, load-carrying and rehabilitation exoskeletons [1].

Assistive exoskeletons are designed to provide a portion of the forces/torques required by the wearer's muscles/joints in performing different tasks. Besides elderlies and patients with joint disease or muscle weakness, the healthy users can also benefit from empowering feature of these robots, resulted from the reduced loads on the wearer's muscles and joints. HAL-3 [2,3], EXPOS [4], LOPES [5,6], RoboKnee [7], Honda's device with stride management assist (SMA) [8] and active pelvis orthosis (APO) [9] are some samples of assistive category of exoskeletons.

Different control algorithms, termed as assistive controllers, are proposed for the assistive category of exoskeletons. Some of these methods provide assisting forces according to the muscles or joints efforts, measured through EMG sensors, as in HAL-3 [2,3] and in [10–12]. Some methods use an approximate value of

* Correspondence to: Ferdowsi University of Mashhad, Azadi Sq., P.O. Box: 9177948974, Mashhad, Iran.

E-mail addresses: Iman.Kardan@stu.um.ac.ir (I. Kardan), Ali_Akbarzadeh@um.ac.ir (A. Akbarzadeh).

http://dx.doi.org/10.1016/j.robot.2017.09.006
0921-8890/

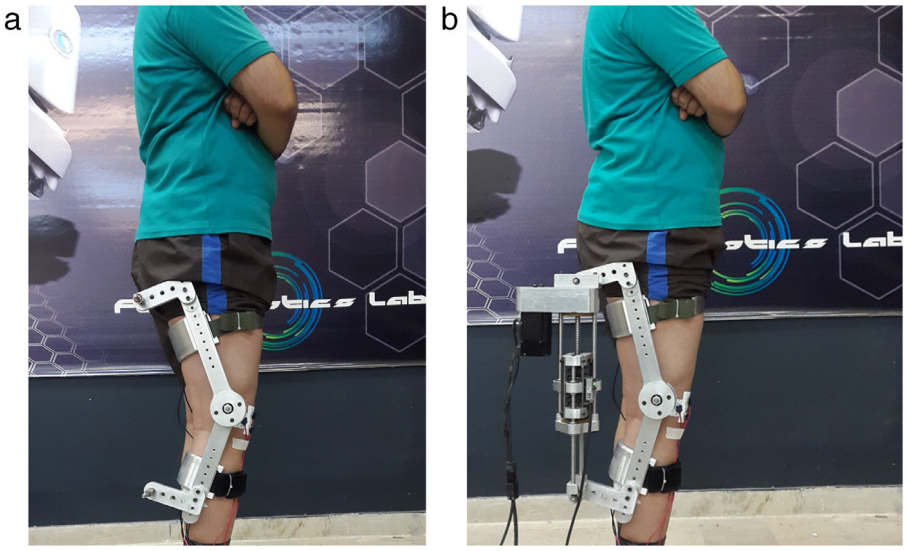

Fig. 1. FUM-KneeExo with foot link detached; (a): Without actuator; (b): Actuated by FUM-LSEA.

joints torques which may be estimated through ground reaction force sensors, as in RoboKnee [7], or estimated through inverse dynamic model of the system [13], or observed by disturbance observer techniques [14–16]. Reducing the apparent impedance of the user's limbs by using force, EMG, or muscle circumference sensors [17–22] and compensating the limbs' inertia [23,24] are other control algorithms proposed for assistive exoskeletons. Adaptive oscillators-based methods [9,25,26] and user's intent estimation algorithms [27–29] are also used in assistive control of exoskeletons.

As note by Nagarajan et al. [30], most of the available assistive algorithms suffer from complexity and requiring an estimation of the user intent. However, a good estimation requires accurate measurements and a precise model of the system dynamics. Therefore, designing simple assistive controllers which are capable of assisting the user, independent from his/her intent, will play an important role in the development of assistive exoskeleton robots.

As a simple and intent-independent assistive method, Nagarajan et al. [30,31] proposed an integral admittance shaping (IAS) algorithm to overcome the limitations in assistive control algorithms. Intent independency, simplicity and the low number of required sensors are interesting features of this method. Moreover, their method does not require force sensors whose drawbacks are well addressed in [15]. However, the IAS algorithm relies on the contact compliance in physical coupling between the exoskeleton and the wearer's body. This compliance is resulted from soft human tissues at the coupling point which is hard to measure and may also change significantly by contraction of the underlying muscles. Moreover, the IAS algorithm requires acceleration feedbacks which suffer from the well-known stability and noise contamination issues with accelerometers or estimated accelerations.

Recently, the authors have proposed a novel assistive controller for compliantly actuated exoskeletons, called output feedback assistive control (OFAC) method [32]. The OFAC method uses inherent characteristics of SEAs and provides numerous advantages over prior assistive controllers. Intent independency, lowest number of required sensors, having a simple model free structure and simplifying the assistive control objective into position control of the SEA motor, are some of the most important features of the OFAC method comparing to the existing assistive control algorithms. Compared to the IAS algorithm, the OFAC method has simpler structure, eliminates the need for acceleration feedback and, more importantly, relies on the compliance of the elastic element of the actuator rather than that of the user tissues. Also, the OFAC method has a lower number of adjustable control coefficients. There are two adjustable coefficients in the OFAC method while the integral admittance shaping algorithm [30,31] has four coefficients. This is a useful property for real-world dynamic systems where the parameter values can only be determined approximately. The semi-optimal control parameters are obtained based on the approximated parameter values. Then the control performance is improved by the fine adjustment of the control coefficients in practice. The small number of adjustable control coefficients simplifies the process of the experimental fine adjustment of the coefficients.

The OFAC parameters are defined through a constrained optimization problem of increasing the integral admittance of the user limbs subjected to comfort, stability and coupled stability constraints. In this paper, H_∞ robustness analysis is used to define additional constraints to assure the robust stability and the robust performance of the OFAC method against uncertainties in system parameters. The robust OFAC method is then implemented on a custom made lower limb exoskeleton, called FUM-KneeExo. FUM-KneeExo is an assistive lower limb exoskeleton with a detachable foot link which is primarily designed to assist the knee motions [33]. The main structure of FUM-KneeExo consists of three articulated links, correspondingly called thigh, shank and foot links. The links are connected through two revolute joints which provide flexion/extension movements for the knee joint and plantar/dorsiflexion movements for the ankle joint. One strap is considered on each link of the robot to secure the links to the corresponding limbs of the user.

When comes into contact with the ground, the foot link transfers the human and exoskeleton weight to the ground. The foot link also contains four force sensors to measure the ground reaction forces. In this paper, the performance of the robust OFAC method is evaluated in a special type of motion, called VSwing motion, in which the foot does not come into contact with the ground. Moreover, the OFAC method does not require any feedback from ground reaction forces. Therefore, there is no need to the foot link of the robot. FUM-KneeExo, with its foot link detached, is worn by a healthy user and the knee loads are measured in two sets of assisted and unassisted motions (see Fig. 1).

As shown in Fig. 1(b), FUM-KneeExo is actuated by a series elastic actuator called FUM-LSEA, built in robotics lab of Ferdowsi university of Mashhad [32,33]. The actuator is attached between thigh and shank links of the robot to generate assistive torques

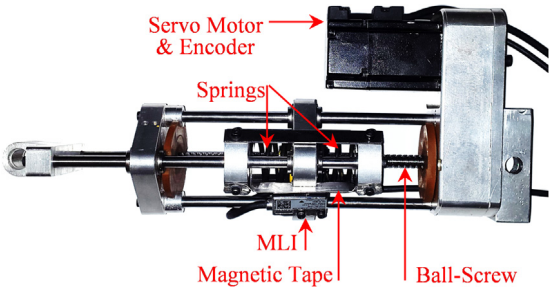

Fig. 2. FUM-LSEA.

for the knee joint. As Fig. 2 illustrates, the actuation force of FUM-LSEA is provided via an ECMA-B2 type 200 (W) AC servo motor, by Delta electronics, with a rated speed of 3000 (rpm). The rotary motion of the servo motor is converted to the linear motion of the actuator through a ball-screw mechanism. A belt and pulley system with a transmission ratio of 2:1 is used to transfer motions from the servo motor to the ball-screw mechanism and also to increase the motor torque. Two springs are put around the screw shaft of the ball-screw mechanism to provide the required compliance for the actuator. The springs operate in parallel with each other and in series with the actuator's motor and its output link. A magnetic linear incremental encoder (MLI) is used to measure the deflection of the springs. The built in incremental encoder of the servo motor measures the motor rotation and consequently the displacement of the nut of the ball-screw.

The rest of the paper is organized as follows; Section 2 provides an introduction to the OFAC method. Robust stability and robust performance constraints for the OFAC method are derived in general form in Section 3. Dynamic model of a special single-DOF human motion (VSwing motion) is derived, verified and then linearized in Section 4. Sections 5 and 6 provide the nominal stability, coupled stability and the robustness constraints, specifically for the human–exoskeleton system in VSwing motion. Section 7 provides the results of evaluating the performance of the robust OFAC method in simulation and practice. Finally, Section 8 concludes the paper.

2. Brief introduction of the OFAC method

To improve the readability of the manuscript, a brief introduction to the OFAC method [32] is provided in this section. The OFAC control law adjusts the desired SEA motor position, x_{md}, as

$$x_{md} = \alpha x_h + \beta \dot{x}_h = \alpha \vartheta \theta_h + \beta \vartheta \dot{\theta}_h, \tag{1}$$

where α and β are the control coefficients and x_h and $\dot{x}_h$ are the change in the SEA length and its rate. θ_h is the joint angle and the constant ϑ relates the changes in the joint angle to the changes in the SEA length in the linearized model of the system, $x_h = \vartheta\theta_h$. Clearly, in linearized models, the constant ϑ also converts the output force of the SEA to an equivalent torque applied to the system, $\tau_e = \vartheta F_e$.

Considering the SEA motor as an ideal position source, i.e. $x_m = x_{md}$, Fig. 3 depicts the block diagram of the OFAC method, where τ_h^a is the torque applied by the human joint while assisted by the exoskeleton and K_s and B_s are the stiffness and damping of the SEA spring. Note that the internal dynamics of the actuator are neglected, assuming that the position control loop of the SEA has a bandwidth sufficiently higher than the maximum frequency of possible human motions.

In Fig. 3, $\hat{Y}_h^u(s)$ is the integral admittance (IA) of the unassisted system and $L_h^a(s)$ is the loop gain given by

$$L_h^a(s) = \left(B_s's + K_s'\right)(\beta s + \alpha - 1)\,\hat{Y}_h^u(s) = \mathcal{R}(s)\,\hat{Y}_h^u(s), \tag{2}$$

in which, $\mathcal{R}(s)$ is the feedback gain, $B_s' = \vartheta^2 B_s$ and $K_s' = \vartheta^2 K_s$. The IA of the assisted system, $\hat{Y}_h^a(s)$, is the closed loop transfer function from τ_h^a to θ_h, calculated as,

$$\hat{Y}_h^a(s) = \frac{\hat{Y}_h^u(s)}{1 - \mathcal{R}(s)\,\hat{Y}_h^u(s)}. \tag{3}$$

The control coefficients are obtained by solving the constrained optimization problem of Eq. (4). This optimization problem maximizes the assistance ratio, or equivalently minimizes its reciprocal, subjected to some constraints for assuring point assistance, comfort and stability and coupled stability of the assisted system.

$$\underset{\alpha,\beta}{\text{minimize}} \quad \frac{1}{\mathcal{A}(\omega_f)}, \tag{4}$$

$$\text{subject to}: \begin{cases} \mathcal{PA}(\omega) \geq 0 & \forall \omega \in [0 \quad \omega_f] \\ \left| \dfrac{\angle \hat{Y}_h^a(j\omega) - \angle \hat{Y}_h^u(j\omega)}{\angle \hat{Y}_h^u(j\omega)} \right| \leq \delta & \forall \omega \in [0 \quad \omega_f] \\ \hat{Y}_h^a(s) \text{ is stable} \\ \hat{Y}_h^a(s) \text{ is passive}. \end{cases}$$

$\mathcal{A}(\omega_f)$ is the mean assistance ratio, giving the average relative amplification of the integral admittance of the assisted system, $\hat{Y}_h^a(j\omega)$, over that of the unassisted system, $\hat{Y}_h^u(j\omega)$. Note that, Eq. (4) finds the maximum of the mean assistance ratio only on the frequency interval of $\omega \in [0 \quad \omega_f]$ which is the user defined interval over which the assistance should be delivered. The mean assistance ratio is calculated as,

$$\mathcal{A}(\omega_f) = \frac{1}{\omega_f} \int_0^{\omega_f} \max\left(\frac{\left|\hat{Y}_h^a(j\omega)\right| - \left|\hat{Y}_h^u(j\omega)\right|}{\left|\hat{Y}_h^u(j\omega)\right|}, 0 \right) d\omega. \tag{5}$$

The first constraint of Eq. (4) assures assisting over the entire frequency interval. $\mathcal{PA}(\omega)$ is the point assistance ratio which is defined as,

$$\mathcal{PA}(\omega) = \frac{\left|\hat{Y}_h^a(j\omega)\right| - \left|\hat{Y}_h^u(j\omega)\right|}{\left|\hat{Y}_h^u(j\omega)\right|}. \tag{6}$$

The second constraint of Eq. (4) is the comfort condition which maintains a small relative difference between phase angle of the IA of the assisted system, $\angle \hat{Y}_h^a(j\omega)$, and that of the unassisted system, $\angle \hat{Y}_h^u(j\omega)$. The parameter δ defines the permissible phase difference. However, defining a suitable comfort condition for assistive devices needs further studies and will be focused in the future works by the authors.

The third constraints of Eq. (4) imposes the stability condition for the nominal assisted system. Different measures may be used to assess the nominal stability, e.g. evaluating the gain margin of $L_h^a(s)$ or finding the roots locations of $\hat{Y}_h^a(j\omega)$. The fourth condition ensures the coupled stability of the nominal assisted system when it comes into contact with passive environments. This condition may also be assessed using different methods such as evaluating the stability of the system while coupled to the worst environments or checking $\angle \hat{Y}_h^a(j\omega)$ which should be confined to the range of $[-180 \quad 0]$ degrees for all ω [34].

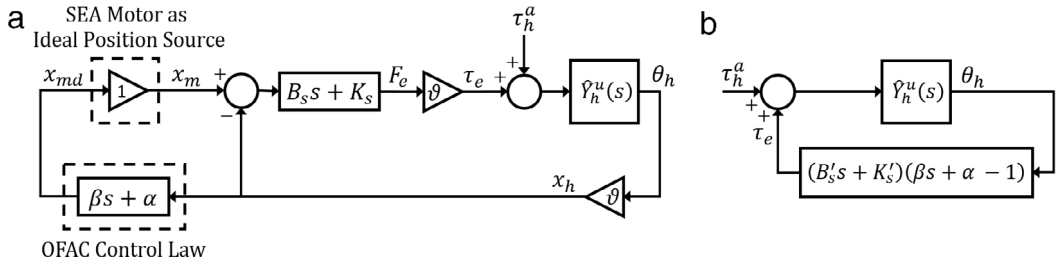

Fig. 3. Block diagram of the OFAC method; (a): Expanded block diagram; (b): Simplified block diagram.

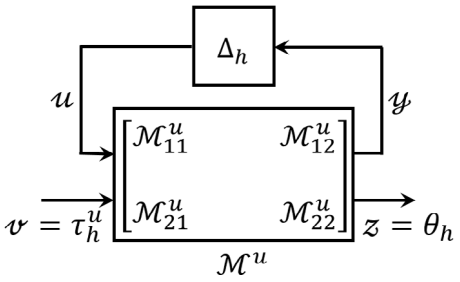

Fig. 4. Standard $\mathcal{M} - \Delta$ configuration for the unassisted human–exoskeleton system.

3. Robustness constraints

The constraints in Eq. (4) ensure stability and successful performance of the OFAC method for the nominal human–exoskeleton system. However, the exact values of the parameters are hard to determine, specifically when human body is part of the system. Therefore, it is necessary to ensure stability of the assisted human–exoskeleton system and satisfactory performance of the OFAC method in the presence of uncertainties. In this paper, H_∞ approach is utilized to obtain robust stability and robust performance constraints.

According to standard H_∞ approach [35], the perturbed system should be re-arranged in a standard $\mathcal{M} - \Delta$ configuration. Fig. 4 shows the standard $\mathcal{M}-\Delta$ configuration for the unassisted human–exoskeleton system where $\mathcal{M}^u$ is the standard transfer matrix of the unassisted system.

In this configuration, Δ_h donates the perturbation block, z is the output vector, v is the exogenous input vector and $\mathcal{M}_{ij}^u$ are the arrays of the transfer matrix $\mathcal{M}^u$. It is clear that $\mathcal{M}_{22}^u = \hat{Y}_h^u$.

As shown in Fig. 5, the OFAC method closes a positive feedback loop around the unassisted system with $\mathcal{R}(s)$ as the feedback gain. Therefore, the standard configuration of the assisted system can be obtained as,

$$\mathcal{M}^a = \begin{bmatrix} \mathcal{M}_{11}^a & \mathcal{M}_{12}^a \\ \mathcal{M}_{21}^a & \mathcal{M}_{22}^a \end{bmatrix}, \tag{7}$$

where,

$$\begin{cases} \mathcal{M}_{11}^a = \mathcal{M}_{11}^u + \mathcal{M}_{12}^u \mathcal{R} \left(1 - \mathcal{M}_{22}^u \mathcal{R}\right)^{-1} \mathcal{M}_{21}^u \\ \mathcal{M}_{12}^a = \mathcal{M}_{12}^u + \mathcal{M}_{12}^u \mathcal{R} \left(1 - \mathcal{M}_{22}^u \mathcal{R}\right)^{-1} \mathcal{M}_{22}^u \\ \mathcal{M}_{21}^a = \left(1 - \mathcal{M}_{22}^u \mathcal{R}\right)^{-1} \mathcal{M}_{21}^u \\ \mathcal{M}_{22}^a = \left(1 - \mathcal{M}_{22}^u \mathcal{R}\right)^{-1} \mathcal{M}_{22}^u. \end{cases} \tag{8}$$

It is clear again that $\mathcal{M}_{22}^a = \hat{Y}_h^a$. This paper considers uncertainties in the system parameters, leading to structured Δ_h blocks. Therefore, structured singular values of the systems, rather than their infinity norms, should be used for robustness analysis [35].

Assuming $\Delta_h(s)$ is normalized, i.e. $|\Delta_h(j\omega)| \leq 1$ for each $\omega \in [0 \quad \infty]$, robust stability of the assisted system in the presence of the uncertainty is guaranteed if the following condition holds,

$$\mu_{\Delta_h}\left(\mathcal{M}_{11}^a\right) \leq 1, \tag{9}$$

where, $\mu_{\Delta_h}\left(\mathcal{M}_{11}^a\right)$ is the structured singular value of $\mathcal{M}_{11}^a$ with respect to $\Delta_h(s)$ and $\mathcal{M}_{11}^a$ is the transfer matrix relating outputs of the uncertainty block to its inputs. Note that, the Δ_h block is not usually normalized and some weighting functions should be included in the system matrix to account for the upper singular value bound of the uncertainty block. Usually, these weighting functions have high-pass filter characteristics since uncertainties in the model increase as the frequency goes up.

In standard $\mathcal{M} - \Delta$ configuration, the robust performance specifications are usually stated in terms of reducing the infinity norm of the transfer matrix from v to z. Considering suitable weighting functions, the norm should be kept below unity for all possible uncertainties. In this manner, the robust performance problem converts to a robust stability problem by assuming a fictitious uncertainty block, Δ_f between z and v. Although Δ_f may be an unstructured uncertainty block, the overall performance uncertainty block, Δ_p, is structured and structured singular values should be used again.

As explained in Section 2, the OFAC method aims at increasing the IA of the assisted system over that of the unassisted system. Therefore, the robust performance of the OFAC method is achieved if $\mathcal{PA}(\omega) \geq \eta$ is achieved for all $\omega \in [0 \quad \omega_f]$ in the presence of all uncertainties in the system parameters. This constraint ensures a minimum of $\eta \times 100$ percent assistance over the desired frequency range and can be equivalently stated as,

$$\begin{aligned} \left\| \frac{\tau_h^a(j\omega)}{\tau_h^u(j\omega)} \right\|_\infty &= \left\| \hat{Y}_h^u(j\omega) \left(\hat{Y}_h^a(j\omega)\right)^{-1} \right\|_\infty \\ &\leq \frac{1}{1+\eta} \quad \forall \omega \in [0 \quad \omega_f]. \end{aligned} \tag{10}$$

However, this constraint should be released for the frequencies above ω_f. This could be achieved by introducing a weighting function and rewriting the Eq. (10) as,

$$\begin{aligned} \left\| W_p(j\omega) \frac{\tau_h^a(j\omega)}{\tau_h^u(j\omega)} \right\|_\infty &= \left\| W_p(j\omega) \hat{Y}_h^u(j\omega) \left(\hat{Y}_h^a(j\omega)\right)^{-1} \right\|_\infty \\ &\leq 1 \quad \forall \omega, \end{aligned} \tag{11}$$

where, $W_p(s)$ is the weighting function with a magnitude of approximately $|W_p(j\omega)| \geq \eta + 1$ for $\omega \in [0 \quad \omega_f]$ and $|W_p(j\omega)| < 1$ for $\omega > \omega_f$. The condition of Eq. (11) can be transformed into the standard form by considering an arrangement of the unassisted and assisted systems as shown in Fig. 6(a). $\mathcal{M}^{-a}$ represents the perturbed integral impedance of the assisted system in standard configuration with $\mathcal{M}_{22}^{-a} = \left(\hat{Y}_h^a\right)^{-1}$ and $\mathcal{M}^o$ represents the standard configuration of the overall system, shown in Fig. 6(b). Performing

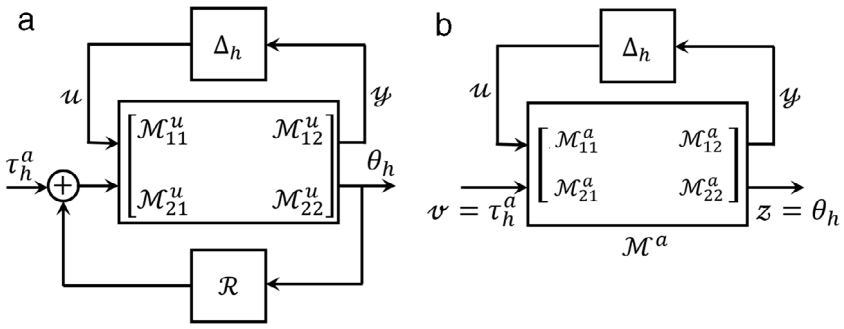

Fig. 5. $\mathcal{M} - \Delta$ configuration of the assisted human–exoskeleton system; (a): Extended diagram; (b): Standard configuration.

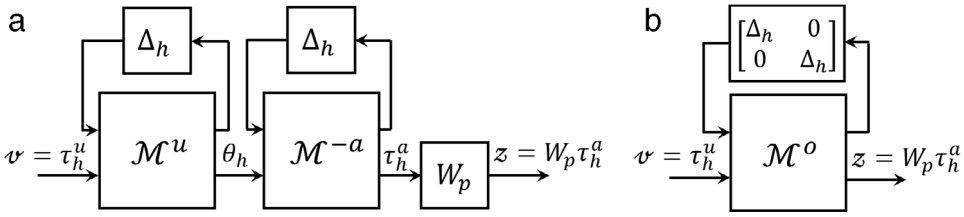

Fig. 6. Robust performance analysis; (a): Arrangement of the unassisted and assisted systems for robust performance analysis; (b): Standard configuration of the overall system for robust performance analysis.

some mathematical calculations, the overall system matrix is obtained as,

$$\mathcal{M}^o = \begin{bmatrix} \mathcal{M}^o_{11} & \mathcal{M}^o_{12} \\ \mathcal{M}^o_{21} & \mathcal{M}^o_{22} \end{bmatrix} \tag{12}$$

$$\begin{cases} \mathcal{M}^o_{11} = \begin{bmatrix} \mathcal{M}^u_{11} & 0 \\ \mathcal{M}^{-a}_{12}\mathcal{M}^u_{21} & \mathcal{M}^{-a}_{11} \end{bmatrix} \\ \mathcal{M}^o_{12} = \begin{bmatrix} \mathcal{M}^u_{12} \\ \mathcal{M}^{-a}_{12}\mathcal{M}^u_{22} \end{bmatrix} \\ \mathcal{M}^o_{21} = W_p \begin{bmatrix} \mathcal{M}^{-a}_{22}\mathcal{M}^u_{21} & \mathcal{M}^{-a}_{21} \end{bmatrix} \\ \mathcal{M}^o_{22} = W_p\mathcal{M}^{-a}_{22}\mathcal{M}^u_{22} \end{cases}$$

Note that, $\mathcal{M}^o_{22} = W_p\mathcal{M}^{-a}_{22}\mathcal{M}^u_{22} = W_p(s)\hat{Y}^u_h(s)\left(\hat{Y}^a_h(s)\right)^{-1}$. Therefore, the robust performance of the OFAC method is guaranteed in the presence of all the parameter uncertainties if,

$$\mu_{\Delta_p}\left(\mathcal{M}^o\right) \leq 1 \tag{13}$$

where, $\Delta_p = blkdiag\left(\Delta_h, \Delta_h, \Delta_f\right)$. Considering the robustness conditions, the coefficients of the robust OFAC can be obtained by solving the following constrained optimization problem.

$$\underset{\alpha,\beta}{\text{minimize}} \quad \frac{1}{\mathcal{A}(\omega_f)} \tag{14}$$

$$\text{subject to :} \begin{cases} \mathcal{PA}(\omega) \geq 0 & \forall\omega \in \begin{bmatrix} 0 & \omega_f \end{bmatrix} \\ \left| \dfrac{\angle\hat{Y}^a_h(j\omega) - \angle\hat{Y}^u_h(j\omega)}{\angle\hat{Y}^u_h(j\omega)} \right| \leq \delta & \forall\omega \in \begin{bmatrix} 0 & \omega_f \end{bmatrix} \\ \hat{Y}^a_h(s) \text{ is stable} & \\ \hat{Y}^a_h(s) \text{ is passive} & \\ \mu_{\Delta_h}\left(M^a_{11}\right) \leq 1 & \forall\omega \\ \mu_{\Delta_p}\left(M^o\right) \leq 1 & \forall\omega \end{cases}$$

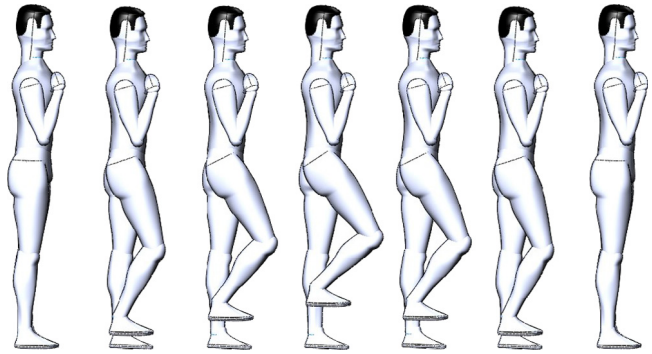

Fig. 7. VSwing cycle.

4. Dynamic modeling

To provide a single-DOF human movement, a special kind of swing motion is defined here which is called vertical swing (VSwing) motion. During the VSwing motion, the user fixes his/her trunk vertically and extends/flexes the knee joint such that the ankle joint is always located vertically with respect to the hip joint. These assumptions make the VSwing a single-DOF motion which can be fully defined by specifying the knee angle. Fig. 7 illustrates some sequences of the VSwing cycle.

4.1. Dynamic model of human–exoskeleton system in VSwing motion

Assuming the straps provide rigid connection between the robot and the user body, the robot links can be considered as parts of the user limbs. Consequently, a simplified model of the assembly of the FUM-KneeExo on the user body, the human–exoskeleton system, is obtained as shown in Fig. 8. The thigh and shank links

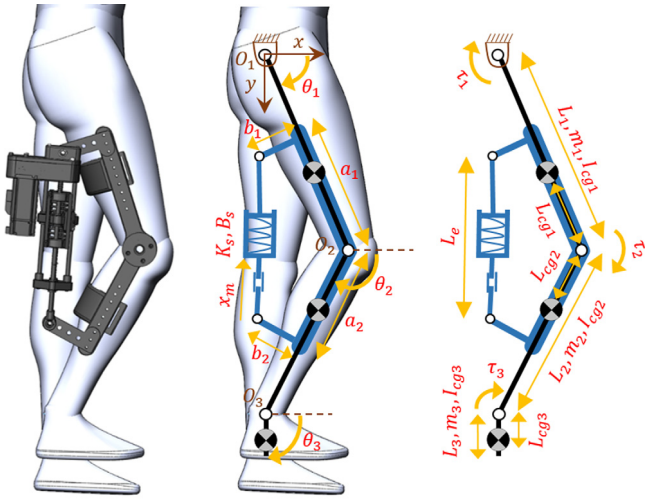

Fig. 8. Kinematic and dynamic parameters of the human–exoskeleton model.

of the model represent the assembly of the respective robot's links and user's limbs. The user's HAT (Head–Arm–Trunk) limb is assumed to be fixed in space during the VSwing motion. Therefore, the human–exoskeleton system is considered to be hinged at the location of the hip joint.

Lagrange formulation is used to derive the dynamic equations of the human–exoskeleton system. Kinematic parameters of the model are defined in Fig. 8. The output force of the SEA, F_e, is obtained as,

$$F_e = K_s\left(\Delta L_e - \Delta x_m\right) + B_s\left(\dot{\Delta L}_e - \dot{\Delta x}_m\right) \tag{15}$$

where ΔL_e is the variation in the FUM-LSEA length from its initial state, L_{e0},

$$\begin{aligned}\Delta L_e = &\left\{\left(b_1\sin\left(\theta_1\right) + a_1\cos\left(\theta_1\right) + a_2\cos(\theta_2) - b_2\sin(\theta_2)\right)^2\right.\\ &\left.+\left(-b_1\cos(\theta_1) + a_1\sin(\theta_1) + a_2\sin(\theta_2) + b_2\cos(\theta_2)\right)^2\right\}^{1/2}\\ &- L_{e0}\end{aligned} \tag{16}$$

and Δx_m is the displacement of the SEA motor from its initial state. It is assumed that in the initial equilibrium state, the SEA motor is located such that the spring is not deflected. Therefore, $\Delta x_m = x_m$.

Considering the clockwise rotation as the positive direction for the angular variables and writing the forward kinematic equations, the x and y coordinates of the center of mass (CM) of the links, x_{cgi} and y_{cgi}, can be easily calculated as functions of the link lengths and the joint angles. The CM velocities along x and y axis, $\dot{x}_{cgi}$ and $\dot{y}_{cgi}$, are obtained by calculating the time derivative of the CM coordinates. Then the kinetic energy of each link, T_i, and the total kinetic energy of the human–exoskeleton system, T_t, are calculated as,

$$\begin{cases} T_i = \dfrac{1}{2}m_i\left(\dot{x}_{cgi}^2 + \dot{y}_{cgi}^2\right) + \dfrac{1}{2}I_{cgi}\dot{\theta}_i^2 \\ T_t = \displaystyle\sum_i T_i \end{cases} \qquad i = 1, 2, 3. \tag{17}$$

where I_{cgi} is the moment of inertia of each segment about an axis perpendicular to the sagittal plane and passing through the CM. The potential energy stored in the SEA spring, U_s, is obtained as,

$$U_s = \frac{1}{2}K_s(\Delta L_e - \Delta x_m)^2 = \frac{1}{2}K_s(\Delta L_e - x_m)^2 \tag{18}$$

The gravitational potential energy of each link, U_{gi}, and the total potential energy of the human–exoskeleton system, U_t, are calculated as,

$$\begin{cases} U_{gi} = -m_i g y_{cgi} \\ U_t = U_s + \displaystyle\sum_i U_{gi} \end{cases} \qquad i = 1, 2, 3. \tag{19}$$

Note that the kinetic and potential energies are derived based on the four variables, θ_1, θ_2, θ_3 and x_m. However, x_m is determined by the OFAC method and considered as a known external input to the system. Therefore, the Lagrangian formulation can be used to obtain the dynamic equations of the system based on the three angular variables as,

$$\frac{d}{dt}\left(\frac{\partial L_t}{\partial \dot{q}_i}\right) + \frac{\partial L_t}{\partial q_i} = Q_i \quad i = 1, 2, 3 \tag{20}$$

where, $L_t = T_t - U_t$ is the scalar Lagrangian function, $\boldsymbol{q} = \{q_1, q_2, q_3\}^T = \{\theta_1, \theta_2, \theta_3\}^T$ is the vector of generalized coordinates and $\boldsymbol{Q} = \{Q_1, Q_2, Q_3\}^T$ is the vector of generalized forces. The generalized forces are determined by calculating the total virtual work done by the external loads during infinitesimal virtual displacements of the generalized coordinates as,

$$\begin{aligned}\delta W_t = &\tau_1\delta\theta_1 + \tau_2\left(\delta\theta_2 - \delta\theta_1\right) + \tau_3\left(\delta\theta_3 - \delta\theta_2\right) - B_1\dot{\theta}_1\delta\theta_1\\ &-B_2\left(\dot{\theta}_2 - \dot{\theta}_1\right)\left(\delta\theta_2 - \delta\theta_1\right) - B_3\left(\dot{\theta}_3 - \dot{\theta}_2\right)\left(\delta\theta_3 - \delta\theta_2\right)\\ &-B_s\left(\dot{\Delta L}_e - \dot{x}_m\right)\delta\Delta L_e.\end{aligned} \tag{21}$$

Note again that x_m is considered as a known external input to the system and consequently its virtual variation is zero. The generalized forces are obtained by calculating the partial derivative of δW_t with respect to the corresponding generalized coordinates as,

$$Q_i = \frac{\partial \delta W_t}{\partial \delta q_i} \quad i = 1, 2, 3 \tag{22}$$

Calculating all the required elements, Eq. (20) gives three dynamic equations for the human–exoskeleton system. This paper studies the effect of the OFAC method on reducing the required knee torque. Therefore, only the second equation of motion, for $q_2 = \theta_2$, should be considered. However, the remaining equations may be used to calculate the torques required by the ankle and hip joints.

It is assumed that during the VSwing motion the ankle joint is always located vertically with respect to the hip joint such that $x_{O3} = \dot{x}_{O3} = 0$. Therefore, the relation in Eq. (23) holds between θ_1 and θ_2.

$$\theta_1 = \cos^{-1}\left(-\frac{L_2\cos\left(\theta_2\right)}{L_1}\right) \tag{23}$$

Moreover, it is assumed that during the VSwing motion the foot is always kept horizontally. Therefore, $\theta_3 = \pi/2$ and $\dot{\theta}_3 = \ddot{\theta}_3 = 0$. Finally, by applying these assumptions to Eq. (20), the equation of motion of the knee joint during the VSwing motion can be obtained as,

$$\tau_2 = M_2\ddot{\theta}_2 + V_2\left(\dot{\theta}_2, \dot{x}_m, \theta_2, x_m\right) + G_2\left(\theta_2, x_m\right). \tag{24}$$

The developed model is validated by modeling VSwing motion of the human–exoskeleton system in a dynamic analysis software. The robot links are fixed to the corresponding human limbs and simple revolute joints are defined between successive links. The HAT link of the human model is fixed vertically in space to simulate the VSwing motion and also to prevent the model from falling. The joint angles of the left leg of the human model are fixed at the upright standing position. The ankle angle of the right leg is set to

Table 1
Parameters values for the human–exoskeleton system.

Thigh & Hip		Shank & Knee		Foot & Ankle		FUM-LSEA	
I^h_{cg1} (kg m^2)	0.503	I^h_{cg2}(kg m^2)	0.383	I^h_{cg3} (kg m^2)	0.025	K_s $\left(\frac{N}{m}\right)$	8600
I^e_{cg1} (kg m^2)	0.023	I^e_{cg2} (kg m^2)	0.013	I_{cg3} (kg m^2)	0.025	B_s $\left(\frac{N\,m\,s}{rad}\right)$	2.56
I_{cg1} (kg m^2)	0.547	I_{cg2} (kg m^2)	0.399	B^h_3 $\left(\frac{N\,m\,s}{rad}\right)$	0.3		
B^h_1 $\left(\frac{N\,m\,s}{rad}\right)$	3.75	B^h_2 $\left(\frac{N\,m\,s}{rad}\right)$	1.05	B_3 $\left(\frac{N\,m\,s}{rad}\right)$	0.3		
B_1 $\left(\frac{N\,m\,s}{rad}\right)$	3.75	B^e_2 $\left(\frac{N\,m\,s}{rad}\right)$	0.5	m^h_3 (kg)	1.45		
m^h_1 (kg)	2.4	B_2 $\left(\frac{N\,m\,s}{rad}\right)$	1.55	m_3 (kg)	1.45		
m^e_1 (kg)	10.1	m^h_2 (kg)	4.7	L_3 (m)	0.07		
m_1 (kg)	12.5	m^e_2 (kg)	1.95	L^h_{cg3} (m)	0.03		
L_1 (m)	0.441	m_2 (kg)	6.65	L_{cg3} (m)	0.03		
a^e_1 (m)	0.3	L_2 (m)	0.443				
b^e_1 (m)	0.05	a^e_2 (m)	0.25				
L^h_{cg1} (m)	0.191	b^e_2 (m)	0.05				
L^e_{cg1} (m)	0.294	L^h_{cg2} (m)	0.192				
L_{cg1} (m)	0.212	L^e_{cg2} (m)	0.144				
		L_{cg2} (m)	0.178				

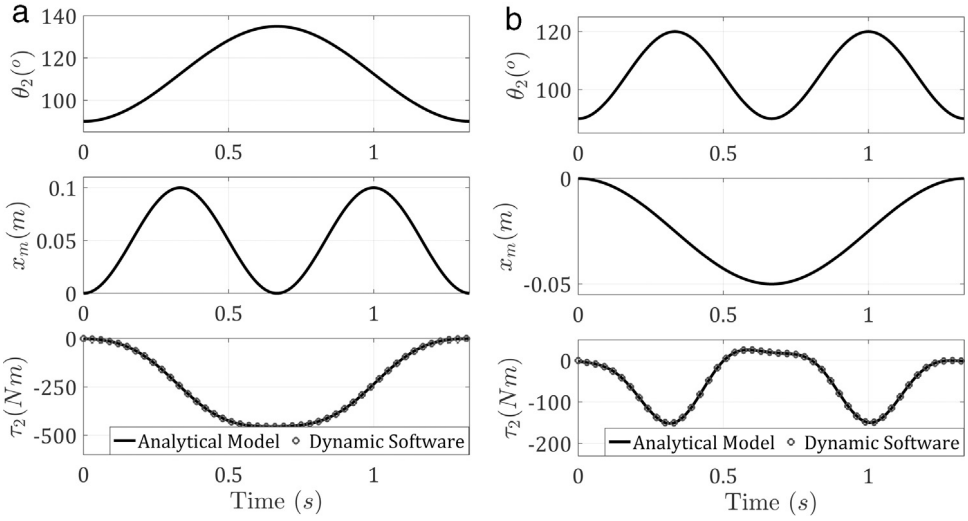

Fig. 9. Verification of the dynamic model; (a): First trajectory, (b): Second trajectory.

hold the sole always horizontally while the desired trajectories are applied to the knee and hip angles of the right leg.

Table 1 gives the values of the dynamic parameters of the human–exoskeleton system used in simulations and experiments. The human parameters are chosen as an average of the dynamic parameters reported for male adults with 1.80 (m) heights and weights of about 100 (kg) [36,37]. The dynamic parameters of the FUM-KneeExo are obtained from their CAD model accompanied by rough measurements and simple identification procedures.

In Table 1, the superscript h indicates the parameters of the human body, the superscript e indicates the parameters of the exoskeleton robot and the parameters without superscript are those of the overall human–exoskeleton system.

In order to validate the dynamic model, the displacement and angular trajectories of Fig. 9 are respectively applied to the SEA motor and the knee angle of the right leg to which the exoskeleton is attached. Note that the hip angle is calculated as $\theta_1 = \cos^{-1}(-L_2/L_1 \cos(\theta_2))$.

Fig. 9 also compares the knee torque trajectories calculated from the analytical model with those obtained from the dynamic modeling software. The very good agreement between the torque trajectories validates the analytical model.

4.2. Linearizing the human–exoskeleton model

Considering the upright standing condition as the initial equilibrium state and assuming low velocities and small displacements, the variables of the human–exoskeleton model can be approximated as,

$$\begin{cases} \theta_2 = \dfrac{\pi}{2} + \tilde{\theta}_2, \\ \sin(\theta_2) = \cos\left(\tilde{\theta}_2\right) \approx 1, \\ \tilde{\theta}_1 = -L_2/L_1\tilde{\theta}_2, \\ \theta_h = \theta_2 - \theta_1 = \tilde{\theta}_2 - \tilde{\theta}_1 \approx (L_1 + L_2)/L_1\tilde{\theta}_2, \\ L_{e0} = \left((a_1 + a_2)^2 + (b_1 - b_2)^2\right)^{1/2}, \\ x_h = \widetilde{\Delta L}_a = -\dfrac{1}{L_{e0}}(a_1 b_2 + a_2 b_1)\theta_h = \vartheta\theta_h, \end{cases} \tag{25}$$

in which, $\tilde{*}$ denotes small changes in the corresponding parameters from their initial state. Finally, the roughly linearized 1-DOF equation of motion of the human–exoskeleton system is obtained as,

$$\begin{aligned} \tau_h = \tau_2 = {} & M_h^u\ddot{\theta}_h + \left(V_h^u + \vartheta^2 B_s\right)\dot{\theta}_h \\ & + \left(G_h^u + \vartheta^2 K_s\right)\theta_h - \vartheta B_s\dot{x}_m - \vartheta K_s x_m, \end{aligned} \tag{26}$$

where,

$$\begin{cases} M_h^u = \dfrac{\left(I_{cg2} + m_2 L_{cg2}^2 - m_2 L_2 L_{cg2}\right)L_1}{(L_1 + L_2)}, \\ V_h^u = B_2, \\ G_h^u = \dfrac{\left(m_2 L_{cg2} + m_3 L_2\right)gL_1}{(L_1 + L_2)}, \\ \vartheta = -\dfrac{1}{L_{e0}}(a_1 b_2 + a_2 b_1), \end{cases} \tag{27}$$

Implementing the OFAC control law of Eq. (1), the position of the SEA motor would be adjusted as,

$$x_m = \alpha\vartheta\theta_h + \beta\vartheta\dot{\theta}_h. \tag{28}$$

Substituting Eq. (28) in Eq. (26), the apparent IA of the human–exoskeleton system, assisted by the OFAC method, is obtained as,

$$\hat{Y}_h^a(s) = \frac{1}{M_h^a s^2 + V_h^a s + G_h^a}, \tag{29}$$

where,

$$\begin{cases} M_h^a = M_h^u - \beta B_s', \\ V_h^a = V_h^u - \beta K_s' - (\alpha - 1)B_s', \\ G_h^a = G_h^u - (\alpha - 1)K_s', \\ B_s' = \vartheta^2 B_s, \\ K_s' = \vartheta^2 K_s. \end{cases} \tag{30}$$

Note that the IA of the unassisted human–exoskeleton system without the compliant actuator is given as,

$$\hat{Y}_h^u(s) = \frac{1}{M_h^u s^2 + V_h^u s + G_h^u}. \tag{31}$$

5. Nominal stability and coupled stability constraints

Considering the root locus of the assisted system, the nominal stability conditions can be easily obtained as,

$$\begin{cases} \alpha \le 1 + \dfrac{\overline{G}_h^u}{K_s'}, \\ \beta \le \min\left\{\dfrac{\overline{V}_h^u - B_s'(\alpha - 1)}{K_s'}, \dfrac{\overline{M}_h^u}{B_s'}\right\}, \end{cases} \tag{32}$$

where, $\bar{*}$ denotes nominal values of corresponding coefficients. According to [34], if an LTI plant remains stable when coupled to the "worst environments", it will have the coupled stability property when contacting any passive environment. The so-called worst environments are composed of pure masses or pure springs and exactly add ±90 degrees of phase lag to the system. However, in the case of a single-DOF system, coupling to a mass or a spring is equivalent to increasing the mass or stiffness of the system, respectively. Considering Eq. (32), the added mass or stiffness will only increase the upper limit of the permissible range of the controller coefficients. Therefore, Eq. (32) gives the necessary and sufficient conditions for the stability and coupled stability of the nominal assisted human–exoskeleton system.

6. Robustness constraints

Regarding the fact that some levels of uncertainties may exist in the parameters of the human–exoskeleton system, the robust stability and performance constraints for the OFAC method are derived in this section. The coefficients of the IA of the unassisted human–exoskeleton system are assumed to be perturbed as,

$$\begin{cases} M_h^u = \overline{M}_h^u\left(1 + p_M(s)\delta_M\right), \\ V_h^u = \overline{V}_h^u\left(1 + p_V(s)\delta_V\right), \\ G_h^u = \overline{G}_h^u\left(1 + p_G(s)\delta_G\right), \end{cases} \tag{33}$$

where, $\bar{*}$ is the nominal coefficient value, δ_* is an uncertain value in the range of $-1 \le \delta_* \le 1$ and $p_*(s)$ is the weighing function governing the upper bound of uncertainty in each coefficient. Considering the uncertain IA coefficients, the state space model of the perturbed unassisted system, in standard $\mathcal{M} - \Delta$ configuration, can be obtained as [35],

$$\begin{cases} \begin{Bmatrix} \dot{x}_1 \\ \dot{x}_2 \end{Bmatrix} = \begin{bmatrix} 0 & 1 \\ -\dfrac{\overline{G}_h^u}{\overline{M}_h^u} & -\dfrac{\overline{V}_h^u}{\overline{M}_h^u} \end{bmatrix}\begin{Bmatrix} x_1 \\ x_2 \end{Bmatrix} \\ \qquad + \begin{bmatrix} 0 & 0 & 0 & 0 \\ -p_M & -\dfrac{p_V}{\overline{M}_h^u} & -\dfrac{p_G}{\overline{M}_h^u} & \dfrac{1}{\overline{M}_h^u} \end{bmatrix}\begin{Bmatrix} u_M \\ u_V \\ u_G \\ \tau_h^u \end{Bmatrix}, \\ \begin{Bmatrix} y_M \\ y_V \\ y_G \\ \theta_h \end{Bmatrix} = \begin{bmatrix} -\dfrac{\overline{G}_h^u}{\overline{M}_h^u} & -\dfrac{\overline{V}_h^u}{\overline{M}_h^u} \\ 0 & \overline{V}_h^u \\ \overline{G}_h^u & 0 \\ 1 & 0 \end{bmatrix}\begin{Bmatrix} x_1 \\ x_2 \end{Bmatrix} \\ \qquad + \begin{bmatrix} -p_M & -\dfrac{p_V}{\overline{M}_h^u} & -\dfrac{p_G}{\overline{M}_h^u} & \dfrac{1}{\overline{M}_h^u} \\ 0 & 0 & 0 & 0 \\ 0 & 0 & 0 & 0 \\ 0 & 0 & 0 & 0 \end{bmatrix}\begin{Bmatrix} u_M \\ u_V \\ u_G \\ \tau_h^u \end{Bmatrix}, \\ \begin{Bmatrix} u_M \\ u_V \\ u_G \end{Bmatrix} = \Delta_h \begin{Bmatrix} y_M \\ y_V \\ y_G \end{Bmatrix}, \\ \Delta_h = \begin{bmatrix} \delta_M & 0 & 0 \\ 0 & \delta_V & 0 \\ 0 & 0 & \delta_G \end{bmatrix}. \end{cases} \tag{34}$$

Therefore, the standard transfer matrix of the unassisted system is obtained as,

$$\mathcal{M}^u = \begin{bmatrix} \mathcal{M}_{11}^u & \mathcal{M}_{12}^u \\ \mathcal{M}_{21}^u & \mathcal{M}_{22}^u \end{bmatrix}, \tag{35}$$

where,

$$\begin{cases} \mathcal{M}_{11}^{u} = \begin{bmatrix} -\dfrac{\overline{M}_h^u p_M s^2}{\mathcal{D}^u} & -\dfrac{p_V s^2}{\mathcal{D}^u} & -\dfrac{p_G s^2}{\mathcal{D}^u} \\ -\dfrac{\overline{V}_h^u \overline{M}_h^u p_M s}{\mathcal{D}^u} & -\dfrac{\overline{V}_h^u p_V s}{\mathcal{D}^u} & -\dfrac{\overline{V}_h^u p_G s}{\mathcal{D}^u} \\ -\dfrac{\overline{G}_h^u \overline{M}_h^u p_M}{\mathcal{D}^u} & -\dfrac{\overline{G}_h^u p_V}{\mathcal{D}^u} & -\dfrac{\overline{G}_h^u p_G}{\mathcal{D}^u} \end{bmatrix}, \\ \mathcal{M}_{12}^{u} = \begin{bmatrix} \dfrac{s^2}{\mathcal{D}^u} \\ \dfrac{\overline{V}_h^u s}{\mathcal{D}^u} \\ \dfrac{\overline{G}_h^u}{\mathcal{D}^u} \end{bmatrix}, \\ \mathcal{M}_{21}^{u} = \begin{bmatrix} -\dfrac{\overline{M}_h^u p_M}{\mathcal{D}^u} & -\dfrac{p_V}{\mathcal{D}^u} & -\dfrac{p_G}{\mathcal{D}^u} \end{bmatrix}, \\ \mathcal{M}_{22}^{u} = \dfrac{1}{\mathcal{D}^u}, \end{cases} \tag{36}$$

in which, $\mathcal{D}^u = \overline{M}_h^u s^2 + \overline{V}_h^u s + \overline{G}_h^u$. Note that $\mathcal{M}_{22}^u = \hat{Y}_h^u(s)$. The standard system matrix of the assisted system can be calculated from Eq. (8). It is seen that $\mathcal{M}^a$ is obtained as,

$$\mathcal{M}^a = \mathcal{M}^u \frac{\mathcal{D}^u}{\mathcal{D}^a} \tag{37}$$

where, $\mathcal{D}^a = \overline{M}_h^a s^2 + \overline{V}_h^a s + \overline{G}_h^a$ and $\mathcal{M}_{22}^a = \hat{Y}_h^a(s)$. Note that, here the weighting matrix is applied through p_M, p_B and p_G functions which should be chosen as high-pass filters. Therefore, Δ_h block is assumed to be normalized and the robust stability constraint is defined as given in Eq. (9).

The perturbed parameter $M_h^u = \overline{M}_h^u(1 + p_M \delta_M)$ can be represented in standard form as shown in Fig. 10. The perturbed parameters V_h^u and G_h^u can also be represented in the same manner. Therefore, the robust performance constraint can be obtained by forming the system matrix $\mathcal{M}^{-a}$ from the block diagram in Fig. 11 which depicts the perturbed integral impedance of the assisted system,

$$\left(\hat{Y}_h^a\right)^{-1} = M_h^a s^2 + V_h^a s + G_h^a = M_h^u s^2 + V_h^u s + G_h^u - \mathcal{R}(s) \tag{38}$$

It is easy to verify that,

$$\mathcal{M}^{-a} = \begin{bmatrix} \mathcal{M}_{11}^{-a} & \mathcal{M}_{12}^{-a} \\ \mathcal{M}_{21}^{-a} & \mathcal{M}_{22}^{-a} \end{bmatrix}, \tag{39}$$

where,

$$\begin{cases} \mathcal{M}_{11}^{-a} = 0_{3\times 3}, \\ \mathcal{M}_{12}^{-a} = \begin{bmatrix} \overline{M}_h^u s^2 \\ \overline{V}_h^u s \\ \overline{G}_h^u \end{bmatrix}, \\ \mathcal{M}_{21}^{-a} = \begin{bmatrix} p_M & p_V & p_G \end{bmatrix}, \\ \mathcal{M}_{22}^{-a} = \mathcal{D}^a. \end{cases} \tag{40}$$

Finally, the overall system matrix is calculated from Eq. (12), the robust performance constraint is obtained from Eq. (13) and the optimal controller coefficients are obtained by solving the constrained optimization problem of Eq. (14).

7. Results and discussions

In this section, performance of the robust OFAC method is evaluated through some simulations and experiments. In the first simulation, controller coefficients are optimized for the linearized human–exoskeleton model from Section 4.2. The controller is then applied to the linear and non-linear models of the human–exoskeleton system. In the second simulation, the performance of the proposed robust OFAC method is compared with the IAS algorithm. Finally, FUM-KneeExo is worn by a healthy subject and the performance of the robust OFAC method, in reducing the loads on the knee muscles, is experimentally evaluated.

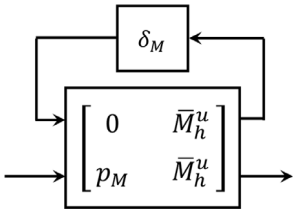

Fig. 10. The perturbed parameter M_h^u in standard form.

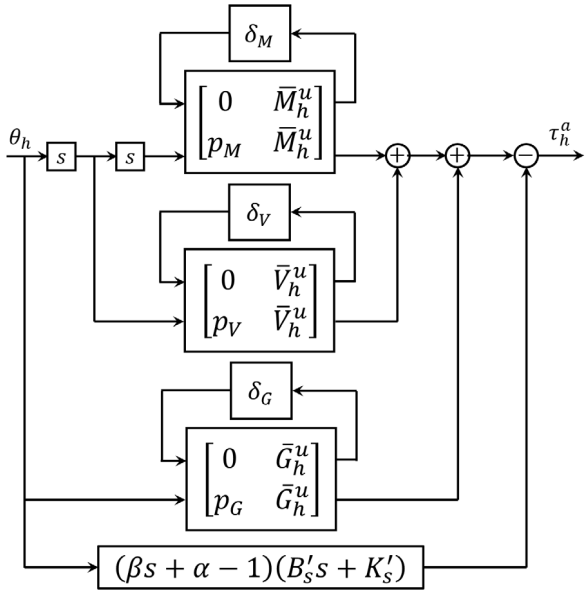

Fig. 11. The perturbed integral impedance of the assisted system.

7.1. Simulation I

In this simulation, the proposed robust OFAC method is applied to the human–exoskeleton system in the VSwing motion. The dynamic model of the system is derived in Section 4 and its parameter values are given in Table 1.

Before finding the optimal controller coefficients, suitable weighing functions should be chosen. In this paper, the uncertainty weighting functions are considered as,

$$p_M(s) = p_V(s) = p_G(s) = \frac{0.5s + 3}{s + 20} \tag{41}$$

This choice indicates a 15% relative uncertainty in each IA coefficient of the unassisted system in low frequencies which goes up to 50% in high frequencies. The frequency response of $p_*(s)$ is shown in Fig. 12. The performance weighting function is chosen as,

$$W_p(s) = \frac{0.1s + 50}{s + 45} \tag{42}$$

This function has a magnitude of about 1.1 over the frequency interval of $\omega \in [0 \quad \omega_f]$ ensuring a minimum of 10% of point assistance in these working frequencies. However, this constraint

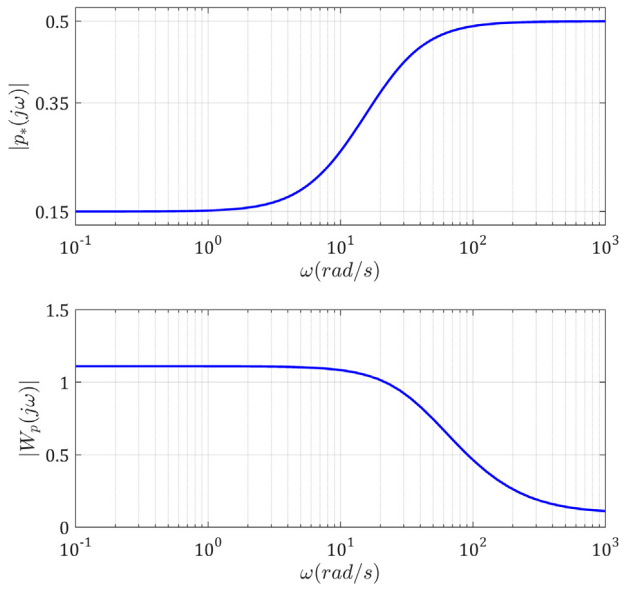

Fig. 12. Magnitude responses of the weighting functions.

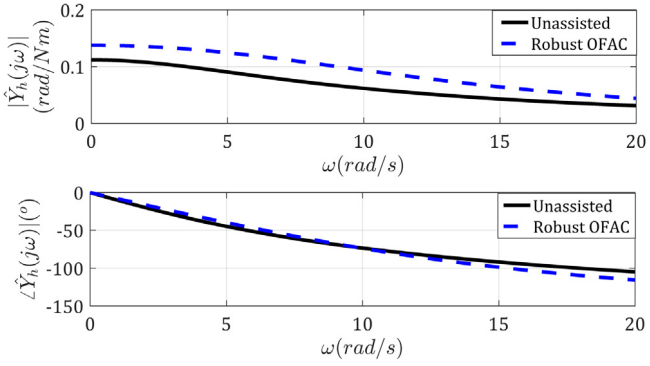

Fig. 13. Comparison of magnitude and phase diagrams of the unassisted and optimally assisted nominal systems.

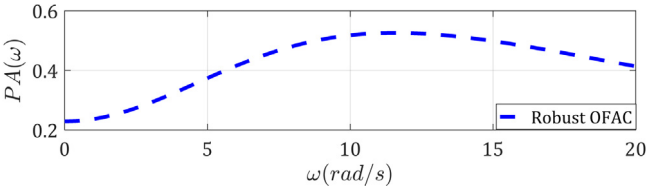

Fig. 14. Point assistance ratio profile for the optimally assisted nominal system.

is released in higher frequencies by the reduction in magnitude of $W_p(s)$. The frequency response of $W_p(s)$ is also depicted in Fig. 12.

Using the parameters values of Table 1 and solving the optimization problem of Eq. (14), the maximum assistance ratio of $\mathcal{A}(\omega_f) = 0.43$ is obtained for $\delta = 0.2$ and $\omega_f = 20$ (rad/s). The optimal controller coefficients are also found to be $\alpha = 1.078$ and $\beta = 0.024$.

The magnitude and phase diagrams of the unassisted and optimally assisted nominal systems are compared in Fig. 13 and the point assistance ratio profile for the optimally assisted nominal system is shown in Fig. 14.

Fig. 13 indicates that the OFAC controller effectively increases the magnitude of the IA of the nominal human–exoskeleton system

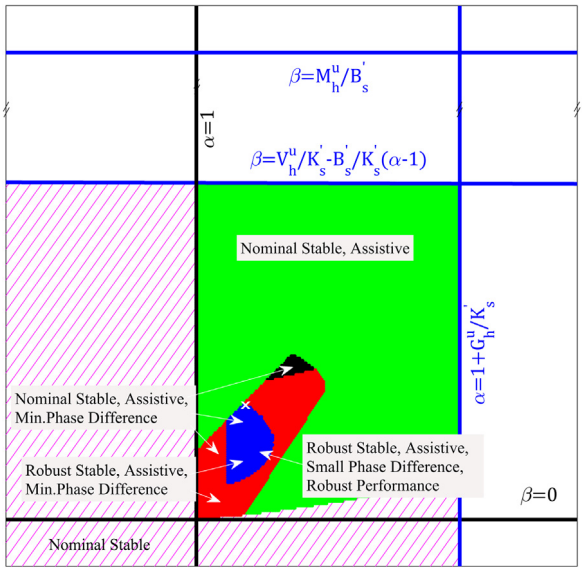

Fig. 15. Permissible regions for selecting the control coefficients.

while maintaining a small phase difference between the assisted and unassisted systems. Moreover, the point assistance ratio profile of Fig. 14 shows that assistance is delivered for all the frequencies of the desired interval. The results also reveal that a maximum assistance is delivered near the natural frequency of the unassisted system

In addition to solving the constrained optimization problem of Eq. (14), a global search is also performed to provide a better sense of the permissible regions for selecting the control coefficients. Fig. 15 visualizes the permissible regions as well as the location of the optimal control coefficients which is indicated by a cross mark. The smallest region in Fig. 15 is called the feasible region in which all the hard constraints of Eq. (14) are satisfied.

Each region in Fig. 15 corresponds to a combination of the hard constraints in Eq. (14). Therefore, relaxing some of the hard constraints will enlarge the permissible regions. For example, Fig. 16 compares the feasible region for the previous case with a case of allowing a maximum resistance of 20% in some frequencies and increasing the permitted phase difference (comfort condition) to 40%. This first case corresponds to $\mathcal{PA}(\omega) \geq 0$ and $\delta = 0.2$ while the second case corresponds to $\mathcal{PA}(\omega) \geq -0.2$ and $\delta = 0.4$. In the second case, the robust performance constraint is correspondingly relaxed by using $0.8W_p(s)$ as the performance weighting function. The cross marks in Fig. 16 indicate the location of the optimal control coefficients for each case.

It is seen that in the second case, where the hard constraints are somewhat relaxed, the feasible region for selecting the control coefficients is enlarged and the maximum assistance ratio is significantly increased to $\mathcal{A}(\omega_f) = 0.93$. However, this extra assistance is obtained at the expense of the user comfort. The permissible phase differences between the required torques for the assisted and unassisted motions are doubled and there may be some resistance against the user motions at some frequencies. In this paper, the priority is given to the user comfort and therefore, $\mathcal{PA}(\omega) \geq 0$ and $\delta = 0.2$ are used in all the simulations and experiments.

The above results are obtained for the nominal model of the human–exoskeleton system. However, the optimal OFAC controller should maintain its performance against uncertainties in model parameters. Fig. 17 shows the diagrams of the structured singular values corresponding to the robust stability and robust

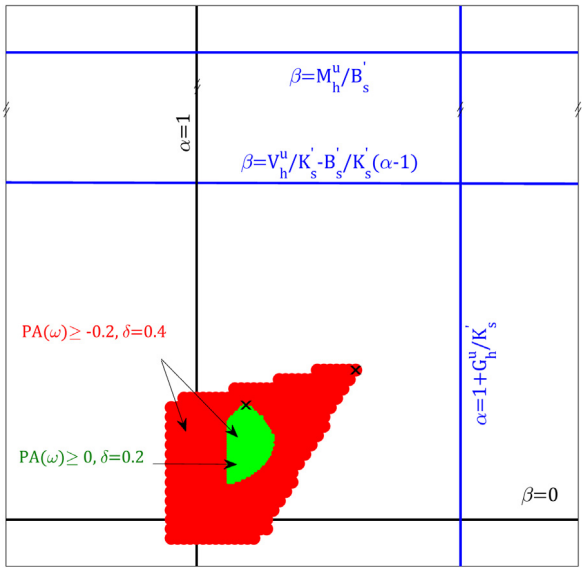

Fig. 16. Effect of relaxing the hard constraints on the feasible region for selecting the control coefficients.

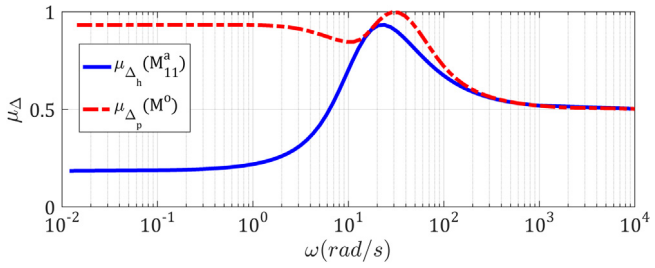

Fig. 17. Structured singular values for robust stability and robust performance conditions.

performance conditions. Both of the singular values are below the unity, indicating that robustness conditions are met. Therefore, for all the considered uncertainties, the optimally assisted system remains stable and receives an amount of assistance over the entire working frequency interval.

The robust performance of the optimal OFAC controller is better demonstrated in Fig. 18. The magnitude responses of the integral admittance of the assisted system are compared with those of the unassisted system for some extreme values of the uncertainty block, $\Delta_h = diag\,(\delta_M, \delta_V, \delta_G)$. As shown in Fig. 18, the integral admittances of the assisted system lie above those of the unassisted system over the entire frequency interval, indicating that assistance is successfully delivered in all the cases.

In order to further verify the effectiveness of the OFAC method, the optimal controller is applied to the nonlinear model of the human–exoskeleton system. The verification process completes in two steps. First, the FUM-LSEA is removed from the model, the angular trajectories of Fig. 19 are applied to the non-linear model and the required knee torques are calculated by solving the inverse dynamic problem. Next, the compliant actuator is added to the model, its motor position is adjusted as governed by the robust OFAC method, the controller coefficients are set as obtained from the linear analysis, the same angular trajectories are applied to the model and the required knee torques are calculated again. Fig. 19 also compares the required knee torques of the unassisted human–exoskeleton system with those of the optimally assisted system.

As shown in Fig. 19, the OFAC method has successfully reduced the required torques of the non-linear model of the human–exoskeleton system while the control coefficients are optimized for the roughly linearized model of the system. Therefore, these results could be regarded as another strong indication of robust performance of the robust OFAC method.

7.2. Simulation II

This simulation evaluates the performance of the robust OFAC method in comparison with the IAS algorithm [30,31]. Table 2 gives the values of the system parameters which are obtained from Ref. [30]. In order to implement the robust OFAC method, the stiffness and damping coefficients of the SEA spring are set identical to the given parameters for the contact compliance.

Eqs. (43) and (44) give the uncertainty and performance weighting functions used for this simulation. Bode diagrams for these weighting functions are depicted in Fig. 20. The considered uncertainty in the system parameters grows from 10% in low frequencies to 15% in high frequencies.

$$p_M\,(s) = p_V\,(s) = p_G\,(s) = \frac{0.15s + 1.5}{s + 15} \tag{43}$$

$$W_p\,(s) = \frac{0.1s + 47}{s + 45} \tag{44}$$

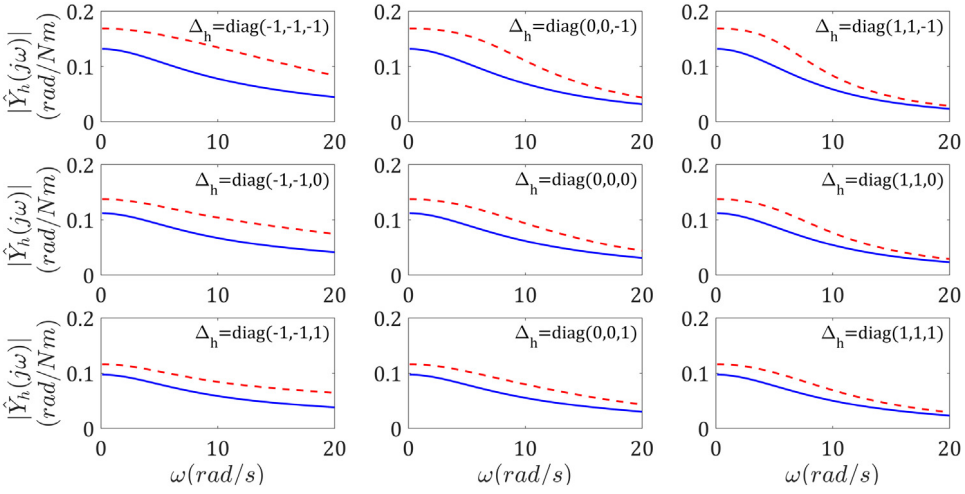

Fig. 18. Evaluation of the robust performance of the optimized robust OFAC method for some extreme uncertainty values; Solid lines: IA magnitude of the unassisted system; Dashed lines: IA magnitude of the assisted system.

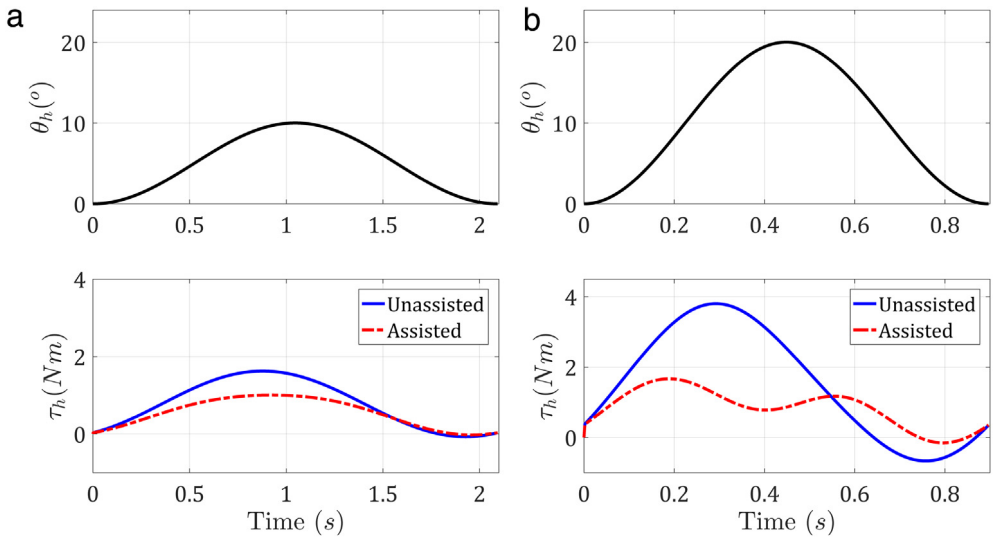

Fig. 19. Performance of the OFAC method in assisting the non-linear human–exoskeleton model; (a): First trajectory; (b): Second trajectory.

Table 2
System parameters used in the second simulation.

Human		Exoskeleton		Overall		Contact/SEA	
$I_h\ (\mathrm{kg\,m^2})$	3.38	$I_e\ (\mathrm{kg\,m^2})$	0.012	$M_h^u\ (\mathrm{kg\,m^2})$	3.392	$K_s = K_c\ (\frac{N}{m})$	1905
$B_h\ (\frac{\mathrm{N\,m\,s}}{\mathrm{rad}})$	3.5	$B_e\ (\frac{\mathrm{N\,m\,s}}{\mathrm{rad}})$	0.013	$V_h^u\ (\frac{\mathrm{N\,m\,s}}{\mathrm{rad}})$	3.513	$B_s = B_c\ (\frac{\mathrm{N\,m\,s}}{\mathrm{rad}})$	9.47
$K_h\ (\frac{Nm}{rad})$	54.7	$K_e\ (\frac{Nm}{rad})$	0.339	$G_h^u\ (\frac{Nm}{rad})$	55.039		

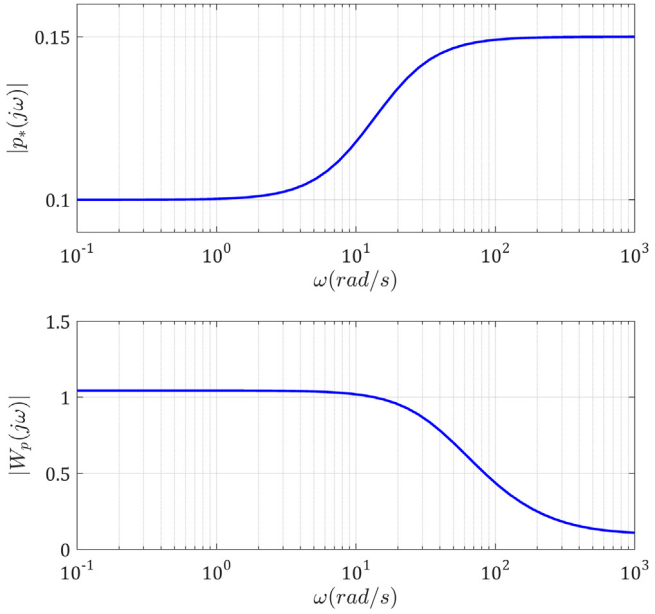

Fig. 20. Magnitude responses of the weighting functions used in the second simulation.

Considering the parameter values in Table 2 and Solving the constrained optimization problem of Eq. (14), the optimal control coefficients for the robust OFAC are obtained as $\alpha = 1.0011$ and $\beta = 0.001$. The maximum assistance ratio by the robust OFAC is found as $\mathcal{A}\left(\omega_f\right) = 0.12$. This is slightly less than the maximum achievable assistance ratio by the IAS algorithm which is reported as $\mathcal{A}\left(\omega_f\right) = 0.14$ in [30,31].

Fig. 21 compares the performance of the two methods for the nominal system. Although the IAS algorithm gives a larger assistance ratio and provides some more assistances in the lower frequencies, the robust OFAC method completely outperforms the IAS algorithm in the frequencies near the natural frequency of the system. By maintaining a very small phase difference between assisted and unassisted systems, maximum comfort is also provided in the same frequency. During lots of normal tasks, like normal walking, body limbs are moved at their natural frequencies to minimize energy consumption [38]. Therefore, this could be a great achievement for the OFAC method to provide maximum assistance with minimum phase shifting in the natural frequencies of the systems.

In order to provide an evaluation of the performance robustness of the two methods, their point assistance profiles are compared in Fig. 22 for some extreme values of the uncertainty block. As shown in Fig. 22, the two methods maintain their successful performances for all the depicted uncertainties. Moreover, in all cases the robust OFAC method provides significantly more assistances in the frequencies near the natural frequency of the system. Fig. 22 also reveals that, despite the variations in the system parameters, the robust OFAC method always provides positive point assistances within the desired frequency interval. However, some small negative point assistances (small resistances) are observed in the case of the IAS method as marked by dotted circles in Fig. 22.

The results provided in this simulation confirm that the robust OFAC method can provide a performance comparable to that of the IAS algorithm. The important point is that this successful performance is achieved with fewer sensors and less number of adjustable control coefficients.

7.3. Experiment

To evaluate the practical performance of the OFAC method, FUM-KneeExo is worn by a male user of 1.80 (m) height and

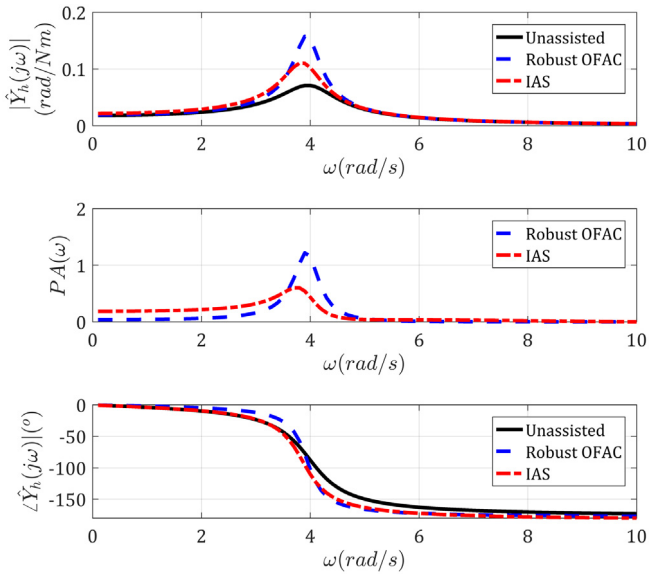

Fig. 21. Magnitude, phase and point assistance ratio diagrams of the robust OFAC method versus those of the IAS algorithm, applied to the nominal system.

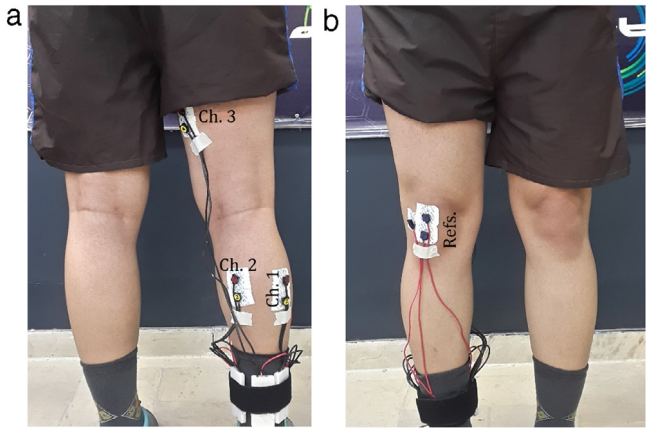

Fig. 23. The location of sEMG electrodes; (a): Signal electrodes; (b): Reference electrodes.

100 (kg) weight. The sEMG signals of the main knee muscles are monitored as an activity measure of the corresponding muscles. By successful implementation of the OFAC method, the knee loads should be reduced and the muscles activities should be decreased.

As shown in Fig. 23, electrodes of the first, second and third sEMG channels are respectively attached to Gastrocnemius Medialis, Gastrocnemius Latralis and Semitendinosus muscles which are three of the main muscles in the knee flexion [39]. The reference electrodes are placed on the patella bone and the sEMG signals are enhanced by shaving the user's skin and cleaning it by alcohol.

The amplified sEMG signals are filtered using a normalized Butterworth filter with a passband frequency of 10 (Hz) to 500 (Hz). The signals are then rectified and their root-mean-square envelopes, $E(n)$, are calculated by considering a moving window of a width of $N = 100$ samples as,

$$E(n) = \sqrt{\frac{1}{N}\sum_{i=0}^{N-1} E_{fr}^2(n-i)} \tag{45}$$

where, E_{fr} represents the filtered rectified version of the raw sEMG signals.

The practical evaluation process is performed in two steps. First, the FUM-LSEA is detached from the FUM-KneeExo, the user is asked to flex/extend his knee according to a desired knee angular trajectory, the sEMG signals of the knee muscles are recorded during the VSwing motion and their envelops are extracted. The desired knee trajectory is a harmonic flexion of the knee joint with an amplitude of 20 degrees and a frequency of 5 radians per second.

Next, the FUM-LSEA is installed and the robust OFAC method is implemented. The user is then asked to follow the same knee angular trajectory by bending/flexing his knee. The sEMG signals are recorded again and their envelopes are extracted. As shown in Fig. 24, in both steps the desired and actual angles of the user's knee are displayed in a monitor in front of the user to achieve more similar trajectories in the two steps.

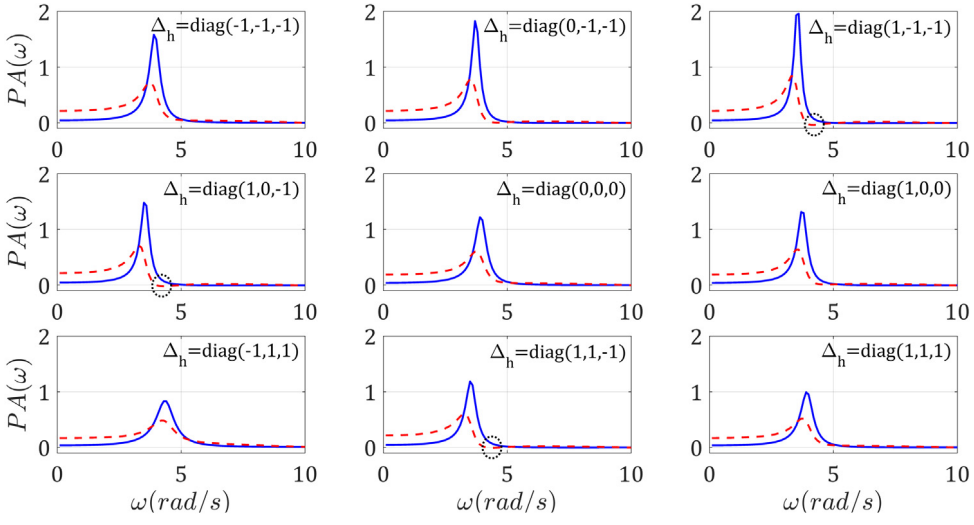

Fig. 22. Comparison of the robust performance of the robust OFAC method with the IAS algorithm for some extreme uncertainty values; Solid lines: Point assistance profile for the OFAC method; Dashed lines: Point assistance profile for the IAS algorithm; Dotted circles: Locations of the small resistances made by the IAS algorithm.

Fig. 24. Healthy subject wearing the FUM-KneeExo.

The filtered sEMG signals are depicted in Fig. 25 while the extracted envelops of the two steps are compared in Fig. 26. Reduced muscles activities are evidently revealed in the sEMG envelope curves of the monitored muscles, especially for the Semitendinosus muscle. This reduction is a clear indication of successful performance of the robust OFAC method in practical conditions.

It is noteworthy that, the change in the SEA length, x_h, is obtained as,

$$x_h = x_m + x_s \tag{46}$$

where, x_m is the motor displacement measured by the motor encoder and x_s is the spring deflection measured by a magnetic linear encoder installed parallel to the spring. The variable $\dot{x}_h$ is estimated through a high gain observer (HGO) whose main equations are given as [40],

$$\begin{cases} \dot{\hat{x}}_1 = \hat{x}_2 + (\gamma/\varepsilon)\left(y - \hat{x}_1\right), \\ \dot{\hat{x}}_2 = \left(\gamma/\varepsilon^2\right)\left(y - \hat{x}_1\right), \\ y = x_1 = x_h \end{cases} \tag{47}$$

in which $y = x_1 = x_h$ is the measured SEA length and $\hat{x}_2 = \dot{\hat{x}}_h$ is an estimation of $\dot{x}_h$. γ and ε are observer gains that determine its transient behavior and chosen as $\gamma = 10$ and $\varepsilon = 0.005$ in these experiments.

8. Conclusion

The main contribution of this paper was to derive robust stability and robust performance constraints for the output feedback assistive control algorithm (OFAC), recently proposed by the authors. Moreover, the practical performance of the robust OFAC algorithm was verified through implementation on a custom made single joint exoskeleton, FUM-KneeExo. The dynamic model of the human–exoskeleton system in a special kind of motion, named as VSwing motion, was derived and then roughly linearized. Adding the robustness constraints to the optimization problem, the linearized model of the human–exoskeleton was used to find

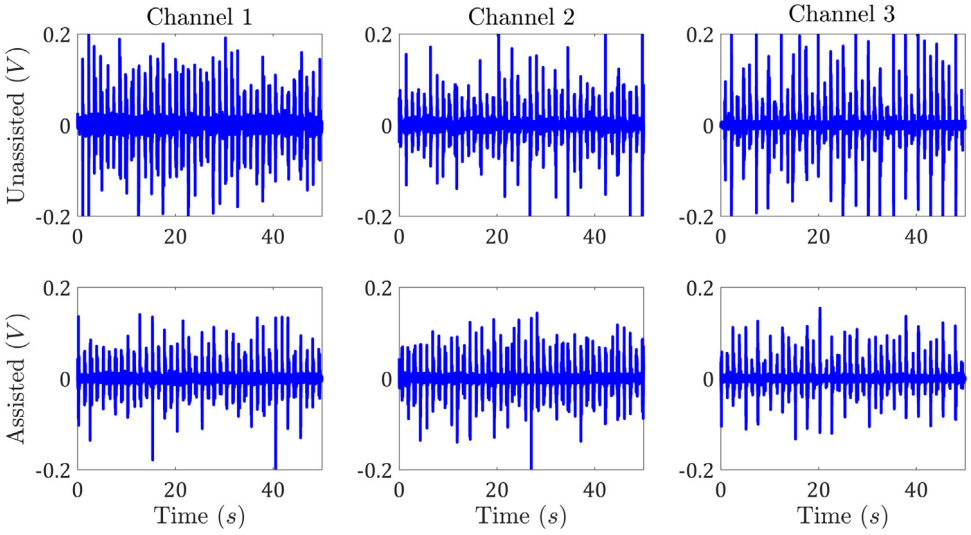

Fig. 25. Filtered sEMG signals during the unassisted and assisted motions.

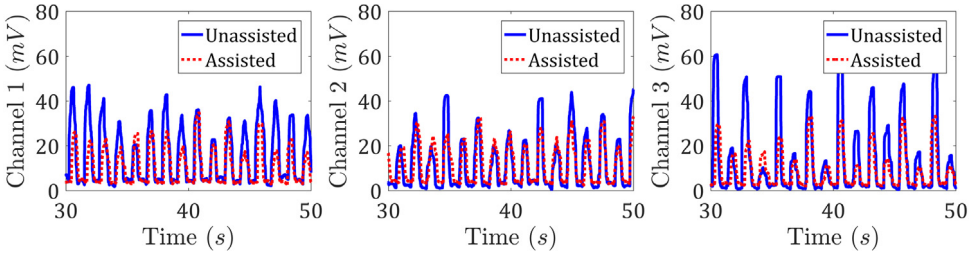

Fig. 26. Comparing the amplitudes of the sEMG envelopes for the unassisted and assisted motions.

the optimal control parameters. The simulation and experimental results clearly showed that including the robustness constraints in the optimization problem, guarantees the robust stability and robust performance of the optimized controller. In spite of the uncertainties in the system, the human–exoskeleton system controlled by the robust OFAC method, remains stable and is assisted by at least a minimum amount. Successful experimental results were obtained by considering a roughly linearized model of the human–exoskeleton system and using only position sensors. The velocity signal is estimated using a high gain observer.

Regarding its practical features, the authors hope that the OFAC method will serve as a building block in assistive control of compliantly actuated exoskeletons and consequently increase the application of compliant actuators in the assistive category of exoskeletons. The OFAC method is currently developed for single joint exoskeletons and its extension to multi-DOF exoskeletons is planned for our future works.

References

[1] T. Yan, M. Cempini, C.M. Oddo, N. Vitiello, Review of assistive strategies in powered lower-limb orthoses and exoskeletons, Robot. Auton. Syst. 64 (2015) 120–136.

[2] D. Lee, M.W. Spong, Passive bilateral teleoperation with constant time delay, IEEE Transactions on Robotics 22 (2) (2006) 269–281.

[3] S. Lee, Y. Sankai, Power assist control for leg with HAL-3 based on virtual torque and impedance adjustment, in: IEEE International Conference on Systems, Man and Cybernetics, vol. 4, 6–9 October 4, 2002.

[4] K. Kong, D. Jeon, Design and control of an exoskeleton for the elderly and patients, IEEE/ASME Trans. Mechatron. 11 (4) (2006) 428–432.

[5] J.F. Veneman, R. Kruidhof, E.E. Hekman, R. Ekkelenkamp, E.H. Van Asseldonk, H. Van Der Kooij, Design and evaluation of the lopes exoskeleton robot for interactive gait rehabilitation, IEEE Trans. Neural Syst. Rehabil. Eng. 15 (3) (2007) 379–386.

[6] H. Vallery, J. Veneman, E.V. Asseldonk, R. Ekkelenkamp, M. Buss, H.V.D. Kooij, Compliant actuation of rehabilitation robots, IEEE Robot. Autom. Mag. 15 (3) (2008) 60–69.

[7] J.E. Pratt, B.T. Krupp, C.J. Morse, S.H. Collins, The RoboKnee: an exoskeleton for enhancing strength and endurance during walking, in: Proceedings of the IEEE International Conference on Robotics & Automation, ICRA '04, 26 April - 1 May, New Orleans, LA, 2004, pp. 2430–2435.

[8] http://asimo.honda.com/innovations/feature/stride-management-assist/.

[9] F. Giovacchini, F. Vannetti, M. Fantozzi, M. Cempini, M. Cortese, A. Parri, T. Yan, D. Lefeber, N. Vitiello, A light-weight active orthosis for hip movement assistance, Robot. Auton. Syst. 73 (2015) 123–134.

[10] J. Rosen, M. Brand, M.B. Fuchs, M. Arcan, A myosignal-based powered exoskeleton system, IEEE Trans. Syst. Humans 31 (3) (2001) 210–222.

[11] H.S. Cheng, M.S. Ju, C.C.K. Lin, Improving elbow torque output of stroke patients with assistive torque controlled by EMG signals, J. Biomech. Eng. 125 (6) (2003) 881–886.

[12] K. Kiguchi, Y. Hayashi, An EMG-based control for an upper-limb power-assist exoskeleton robot, IEEE Trans. Syst. Man Cybern. B 42 (4) (2012) 1064–1071.

[13] S. Hussain, S.Q. Xie, P.K. Jamwal, Adaptive impedance control of a robotic orthosis for gait rehabilitation, IEEE Trans. Cybern. 43 (3) (2013) 1025–1034.

[14] W. Huo, S. Mohammed, Y. Amirat, K. Kong, (2016) Active impedance control of a lower limb exoskeleton to assist sit-to-stand movement, in: IEEE International Conference on Robotics and Automation, ICRA, 16–21 May, 2016, pp. 3530-3536.

[15] S. Oh, K. Kong, Y. Hori, Design and analysis of force-sensor-less power-assist control, IEEE Trans. Ind. Electron. 61 (2) (2014) 985–993.

[16] S. Oh, E. Baek, S.K. Song, S. Mohammed, D. Jeon, K. Kong, A generalized control framework of assistive controllers and its application to lower limb exoskeletons, Robot. Auton. Syst. 73 (2015) 68–77.

[17] Z. Li, Z. Huang, W. He, C.Y. Su, Adaptive impedance control for an upper limb robotic exoskeleton using biological signals, IEEE Trans. Ind. Electron. 64 (2) (2017) 1664–1674. http://dx.doi.org/10.1109/TIE.2016.2538741.

[18] A.M. Khan, D.W. Yun, M.A. Ali, J. Han, K. Shin, C. Han, Adaptive impedance control for upper limb assist exoskeleton, in: IEEE International Conference on Robotics and Automation, ICRA, 26–30 May, 2015, pp. 4359–4366.

[19] K. Kiguchi, S. Kariya, K. Watanabe, K. Izumi, T. Fukuda, An exoskeletal robot for human elbow motion support-sensor fusion, adaptation, and control, IEEE Trans. Syst. Man Cybern. 31 (3) (2001) 353–361.

[20] K. Kiguchi, T. Tanaka, T. Fukuda, Neuro-fuzzy control of a robotic exoskeleton with EMG signals, IEEE Trans. Fuzzy Syst. 12 (4) (2004) 481–490.

[21] A. Morbi, M. Ahmadi, A.D. Chan, R. Langlois, Stability-guaranteed assist-as-needed controller for powered orthoses, IEEE Trans. Control Syst. Technol. 22 (2) (2014) 745–752.

[22] G. Aguirre-Ollinger, J.E. Colgate, M. Peshkin, A. Goswami, Active-impedance control of a lower-limb assistive exoskeleton, in: IEEE 10th International Conference on Rehabilitation Robotics, 13–15 June, Noordwijk, 2007, pp. 188–195.

[23] G. Aguirre-Ollinger, J.E. Colgate, M.A. Peshkin, A. Goswami, Design of an active one-degree-of-freedom lower-limb exoskeleton with inertia compensation, Int. J. Robot. Res. 30 (4) (2011) 486–499.

[24] G. Aguirre-Ollinger, J.E. Colgate, M. Peshkin, A. Goswami, Inertia compensation control of a one-degree-of-freedom exoskeleton for lower-limb assistance: initial experiments, IEEE Trans. Neural Syst. Rehabil. Eng. 20 (1) (2012) 68–77.

[25] R. Ronsse, T. Lenzi, N. Vitiello, B. Koopman, E. van Asseldonk, S.M.M. De Rossi, J. van den Kieboom, H. van der Kooij, M.C. Carrozza, A.J. Ijspeert, Oscillator-based assistance of cyclical movements: model-based and model-free approaches, Med. Biol. Eng. Comput. 49 (2011) 1173–1185.

[26] G. Aguirre-Ollinger, Exoskeleton control for lower extremity assistance based on adaptive frequency oscillators: adaptation of muscle activation and movement frequency, Proc. Inst. Mech. Eng. H 229 (1) (2015) 52–56.

[27] N. Karavas, A. Ajoudani, N. Tsagarakis, J. Saglia, A. Bicchi, D. Caldwell, Tele-impedance based assistive control for a compliant knee exoskeleton, Robot. Auton. Syst. 73 (2015) 78–90.

[28] A.M. Khan, D.W. Yun, M.A. Ali, K.M. Zuhaib, C. Yuan, J. Iqbal, J. Han, K. Shin, C. Han, Passivity based adaptive control for upper extremity assist exoskeleton, Int. J. Control Autom. Syst. 14 (1) (2016) 291–300.

[29] J. Huang, W. Huo, W. Xu, S. Mohammed, Y. Amirat, Control of upper-limb power-assist exoskeleton using a human–robot interface based on motion intention recognition, IEEE Trans. Autom. Sci. Eng. 12 (4) (2015) 1257–1270.

[30] U. Nagarajan, G. Aguirre-Ollinger, A. Goswami, Integral admittance shaping: A unified framework for active exoskeleton control, Robot. Auton. Syst. 75 (2016) 310–324.

[31] U. Nagarajan, G. Aguirre-Ollinger, A. Goswami, Integral admittance shaping for exoskeleton control, in: IEEE International Conference on Robotics and Automation, ICRA, 2015, pp. 5641–5648.

[32] I. Kardan, A. Akbarzadeh, Output feedback assistive control of single-DOF SEA powered exoskeletons, Ind. Robot 44 (3) (2017) 275–287.

[33] K. Kamali, A.A. Akbari, A. Akbarzadeh, Trajectory generation and control of a knee exoskeleton based on dynamic movement primitives for sit-to-stand assistance, Adv. Robot. 30 (13) (2016) 846–860.

[34] J.E. Colgate, The Control of Dynamically Interacting Systems(Doctoral dissertation), Massachusetts Institute of Technology, 1988.

[35] D.W. Gu, P. Petkov, M.M. Konstantinov, Robust Control Design with MATLAB®, Springer Science & Business Media, 2014.

[36] D.A. Winter, Biomechanics and Motor Control of Human Movement, John Wiley & Sons, 2009.

[37] G.C. Agarwal, C.L. Gottlieb, Compliance of the human ankle joint, J. Biomech. Eng. 99 (3) (1977) 166–170.

[38] A.D. Kuo, A simple model of bipedal walking predicts the preferred speed–step length relationship, J. Biomech. Eng. 123 (3) (2001) 264–269.

[39] http://seinam.org/.

[40] L.K. Vasiljevic, H.K. Khalil, Differentiation with high-gain observers the presence of measurement noise, in: IEEE Conference on Decision and Control, 13-15 December, San Diego, CA, 2006, pp. 4717–4722.

Iman Kardan received his B.Sc. and M.Sc. degree in Mechanical Engineering from Amirkabir University of Technology (Tehran Polytechnic), Tehran, Iran in 2008 and 2011, respectively. He is currently a Ph.D. student in Mechanical Engineering Department of Ferdowsi University of Mashhad, Mashhad, Iran. His research interest is in the area of robotics, microrobotics, control and smart materials.

Alireza Akbarzadeh received his Ph.D. in Mechanical Engineering in 1997 from the University of New Mexico in USA. He worked at Motorola, USA, for 15 years where he led R&D as well as automation teams. He joined the Ferdowsi University of Mashhad in 2005 and is currently a full professor in the Mechanical Engineering Department. He has over 45 journal publications and over 60 conference papers. His areas of research include robotics (parallel robots, biologically inspired robots, bipedal robots, and rehabilitation robotics), dynamics, kinematics, control, automation, optimization as well as design and analysis of experiments. He is also a founding member of the Center of Excellence on Soft Computing and Intelligent Information Processing (SCIIP).